Revisiting sterile neutrino dark matter in gauged $U(1)_{B-L}$ model

Shintaro Eijima[*]

ICRR, The University of Tokyo, Kashiwa, Chiba 277-8582, Japan

Osamu Seto[†]

Department of Physics, Hokkaido University, Sapporo 060-0810, Japan

Takashi Shimomura[‡]

Faculty of Education, Miyazaki University, Miyazaki 889-2192, Japan
and Department of Physics, Kyushu University, Fukuoka 819-0395, Japan

We reexamine sterile neutrino dark matter in gauged $U(1)_{B-L}$ model. Improvements have been made by tracing and careful evaluation of the evolution of the number densities of sterile neutrinos N and extra neutral gauge bosons Z'. As a result, the cosmologically-interesting gauge coupling of $U(1)_{B-L}$ for freeze-in sterile neutrinos turns out to be smaller than the values reported in the literature. This avoids the overproduction of Z' so that it is consistent with the big bang nucleosynthesis and the cosmic microwave background constraints on the effective number of neutrino species. Similarly, the free-streaming length constraints exclude a large parameter space derived in previous studies. In addition to known freeze-in pair production of N from the standard model fermion pairs, we find the case that N is dominantly produced from a pair of Z' at the temperature characterized by the $B - L$ breaking scalar mass. Thus, the naive truncation of the $U(1)_{B-L}$ scalar contribution made in the literature is not valid.

I. INTRODUCTION

Not only the existence of nonbaryonic dark matter (DM) but also nonvanishing neutrino masses are major open questions in particle physics and cosmology. Those are also hints and evidence for new physics beyond the Standard Model (SM). One of the simple extensions of the SM to explain those two problems is to introduce right-handed (RH) neutrinos, which are singlets under the SM gauge group. With Majorana masses of RH neutrinos, the tiny neutrino masses can be naturally generated through the seesaw mechanism [1–4]. The resultant heavier-mass eigenstates compared with the active neutrinos responsible for neutrino oscillations are called sterile neutrinos. They slightly mix with the left-handed (LH) components via the active-sterile mixings. The lightest of them is a good candidate for (warm) DM [5] if the lifetime is long enough [6,7].

The νMSM [8,9] is known as an extension with three RH neutrinos including such a sterile neutrino dark matter.

Three generations of RH neutrinos can be theoretically verified, once the SM is extended by introducing an extra $U(1)$ gauge symmetry under which RH neutrinos are charged. Since RH neutrinos are chiral, their charges and generations are determined by gauge anomaly cancellation. A well-studied example is gauged $U(1)_{B-L}$ symmetry [10–12].

If RH neutrinos interact through an extra $U(1)$ gauge interaction, the sterile neutrino DM can be generated effectively. The Dodelson-Widrow (DW) mechanism [13], where sterile neutrino DM is produced through the active-sterile mixings, conflicts with the observations in x-ray [14–18] and for Lyman-α forest (See, e.g., [7] and references therein). Thus, the production from scatterings through new mediators [19–25] is an alternative promising scenario. This class of nonthermal production is sometime called "freeze-in" [26]. For a review, see, e.g., Refs. [27,28]. Nonthermal productions of an extra $U(1)$ gauge interacting sterile neutrino DM have been investigated for a large gauge coupling [19], and for a small gauge coupling in Refs. [20,21,29–33].

The purpose of this paper is to reexamine the freeze-in production of $U(1)_{B-L}$ gauge-interacting sterile neutrino DM. After we examine the production processes of the sterile neutrino N and the extra neutral gauge boson Z' in

[*]eijima@icrr.u-tokyo.ac.jp
[†]seto@particle.sci.hokudai.ac.jp
[‡]shimomura@cc.miyazaki-u.ac.jp

detail and trace the evolution of the number densities of N and Z', we evaluate cosmological constraints on the model from the viewpoint of light degrees of freedom and the structure formation. We find that the inverse decay production of Z' from SM particles in equilibrium is dominant in cases with a very small $U(1)_{B-L}$ gauge coupling. Due to the contribution, the resultant abundances of the sterile neutrino DM and light Z' as dark radiation (DR) are larger than previously estimated. Therefore, the impacts of this increase on the big bang nucleosynthesis (BBN) and the cosmic microwave background (CMB) are estimated, in which constraints on the gauge coupling are obtained. We also find that the contribution from the on shell Z' decay is dominant in the scattering production process through s-channel Z' exchange. Since the produced N from the Z' decay is relativistic, the free-streaming length constraints limit the viable parameter space. Moreover, we find cases where the sterile neutrino DM is dominantly produced by the pair production from a pair of Z'. The cross section of this mode depends on the mass of $U(1)_{B-L}$ breaking scalar. Thus, the naive truncation of the scalar contribution made in literature cannot be validated.

This paper is organized as follows. We describe Langrangian of the model, and read vertices of interactions in Sec. II. After we summarize Boltzmann equations which need to be solved in Sec. III, we consider three production scenarios of the sterile neutrino DM and estimate the DM abundance by taking into account cosmological constraints in Sec. IV. We shortly discuss the implication to dark matter detection in Sec. V. We discuss the conclusion in Sec. VI.

II. MODEL

We consider the extension of the SM by gauging $U(1)_{B-L}$ symmetry, where B and L are the baryon and lepton number, respectively. Under the $SU(3)_C \times SU(2)_L \times U(1)_Y \times U(1)_{B-L}$ gauge groups, three generations of RH neutrinos (ν_R^i with i running over 1,2,3) have to be introduced for the anomaly cancellation. The scalar sector of the SM is also extended by introducing one complex scalar Φ_{B-L}, which is charged under the $U(1)_{B-L}$, to break the extra gauge symmetry spontaneously. This is the minimal extension regarding the gauged $U(1)_{B-L}$ symmetry. In Table I, Q (u_R, d_R) and L (e_R, ν_R) denote the LH (RH) quarks and leptons, respectively.

A. Lagrangian

The Lagrangian is given by

$$\mathcal{L} = \mathcal{L}_{\rm SM} + \mathcal{L}_{\nu_R} + V(\Phi_H, \Phi_{B-L}), \qquad (1)$$

$$\mathcal{L}_{\nu_R} = \overline{\nu_R^i}(iD_\mu\gamma^\mu)\nu_R^i - y_{\nu ij}\overline{L^i}\tilde{\Phi}_H\nu_R^j - \frac{1}{2}y_{\nu_R^i}\Phi_{B-L}\overline{\nu_R^{iC}}\nu_R^i$$
$$+ {\rm H.c.}, \qquad (2)$$

TABLE I. In addition to the SM particle content, three RH neutrinos ν_R^i ($i = 1, 2, 3$) and one $U(1)_{B-L}$ Higgs field Φ_{B-L} are introduced.

	$SU(3)_C$	$SU(2)_L$	$U(1)_Y$	$U(1)_{B-L}$
Q^i	**3**	**2**	$\frac{1}{6}$	$\frac{1}{3}$
u_R^i	**3**	**1**	$\frac{2}{3}$	$\frac{1}{3}$
d_R^i	**3**	**1**	$-\frac{1}{3}$	$\frac{1}{3}$
L^i	**1**	**2**	$-\frac{1}{2}$	-1
e_R^i	**1**	**1**	-1	-1
ν_R^i	**1**	**1**	0	-1
Φ_H	**1**	**2**	$\frac{1}{2}$	0
Φ_{B-L}	**1**	**1**	0	2

where $\mathcal{L}_{\rm SM}$, $\mathcal{L}_{\nu_R}$, and $V(\Phi_H, \Phi_{B-L})$ are Lagrangian of the SM, RH neutrinos, and the scalar potential of this model, respectively. In Eq. (2), the superscript C denotes the charge conjugation of ν_R^i, and $\tilde{\Phi}_H \equiv \epsilon\Phi_H^\dagger$ is the conjugation of the Higgs field Φ with ϵ being the antisymmetric tensor. Yukawa couplings with LH lepton doublets and among RH neutrinos are denoted by y_ν and $y_{\nu_R^i}$ respectively, in which i and j are indices of flavor or generation. We work on the diagonal basis of $y_{\nu_R^i}$ without loss of generality.

Due to the $U(1)_{B-L}$ symmetry, the covariant derivative is modified as

$$D_\mu = \partial_\mu - ig_2 W_\mu - ig_1 Y B_\mu - ig_{B-L}q_{B-L}X_\mu, \qquad (3)$$

where W, B, and X represent the gauge fields, and g_2, g_1, and g_{B-L} are the gauge coupling constants of $SU(2)_L$, $U(1)_Y$, and $U(1)_{B-L}$, respectively. The $U(1)_Y$ and $U(1)_{B-L}$ charges listed in Table I are denoted as Y and q_{B-L}. We omit any symbol about the $SU(3)_C$ color interaction.

There may exist a gauge kinetic mixing term

$$\mathcal{L}_\epsilon = \frac{\epsilon}{2}B_{\mu\nu}X^{\mu\nu}, \qquad (4)$$

where $B_{\mu\nu}$ and $X_{\mu\nu}$ are the gauge field strength of $U(1)_Y$ and $U(1)_{B-L}$ gauge field, respectively, and ϵ is a mixing parameter. The importance of this term has been studied intensively in the context of the so-called dark photon. Since we are interested in the $U(1)_{B-L}$ gauge interaction on RH neutrinos, we concentrate on the cases where the effect of the gauge kinetic mixing is negligible and set ϵ vanishing in this paper.[1]

---

[1]If the gauge kinetic mixing effects are more dominant than the direct gauge interaction, the model would reduce to a dark photon model. For a recent review on the dark photon, see, e.g., Ref. [34].

B. Scalar potential

1. Mass eigenstates and Higgs mixing

We derive the masses of introduced particles with the following scalar potential,

$$
\begin{aligned}
V(\Phi_H, &\Phi_{B-L}) \\
&= \frac{1}{2}\lambda_1\left(|\Phi_H|^2 - \frac{v^2}{2}\right)^2 + \frac{1}{2}\lambda_2\left(|\Phi_{B-L}|^2 - \frac{v_{B-L}^2}{2}\right)^2 \\
&\quad + \lambda_3\left(|\Phi_H|^2 - \frac{v^2}{2}\right)\left(|\Phi_{B-L}|^2 - \frac{v_{B-L}^2}{2}\right),
\end{aligned}
\tag{5}
$$

where all parameters, $\lambda_1, \lambda_2, \lambda_3, v_{B-L}$, and $v \simeq 246$ GeV, are real and positive. At the electroweak and $B-L$ broken vacuum, Φ_H and Φ_{B-L} fields can be expanded around those vacuum expectation values (VEVs) v and v_{B-L}, respectively.

In this vacuum, the $U(1)_{B-L}$ gauge boson X absorbs the corresponding Nambu-Goldstone mode and becomes the massive extra neutral gauge boson Z' with the mass

$$
m_{Z'}^2 = 4g_{B-L}^2 v_{B-L}^2,
\tag{6}
$$

and three RH neutrinos also obtain their Majorana masses

$$
m_{\nu_R^i} = \frac{y_{\nu_R^i}}{\sqrt{2}} v_{B-L}.
\tag{7}
$$

Then, the nonvanishing neutrino masses can be generated through the type-I seesaw mechanism as

$$
m_{\nu ij} = -m_{Dik}\frac{1}{m_{\nu_R^k}}m_{D^{kj}}^T,
\tag{8}
$$

with

$$
m_{Dik} = \frac{y_{\nu ik} v}{\sqrt{2}}.
\tag{9}
$$

The mass eigenstates of the scalars, h and ϕ, are obtained from those physical fluctuations ϕ_H and ϕ_{B-L} in Φ_H and Φ_{B-L}, respectively, as

$$
\begin{pmatrix} \phi_H \\ \phi_{B-L} \end{pmatrix} = \begin{pmatrix} \cos\alpha & \sin\alpha \\ -\sin\alpha & \cos\alpha \end{pmatrix}\begin{pmatrix} h \\ \phi \end{pmatrix},
\tag{10}
$$

with the mixing angle α. Their masses are given by

$$
m_h^2 = \frac{1}{2}\left(\lambda_1 v^2 + \lambda_2 v_{B-L}^2 + \frac{\lambda_1 v^2 - \lambda_2 v_{B-L}^2}{\cos(2\alpha)}\right),
\tag{11a}
$$

$$
m_\phi^2 = \frac{1}{2}\left(\lambda_1 v^2 + \lambda_2 v_{B-L}^2 - \frac{\lambda_1 v^2 - \lambda_2 v_{B-L}^2}{\cos(2\alpha)}\right).
\tag{11b}
$$

At the $\alpha \to 0$ limit, h is reduced to the SM Higgs boson ϕ_H. For a small $\alpha \ll 1$, h and ϕ are identified with the SM-like Higgs boson and the singlet-like scalar, respectively. Thus, we take $m_h \simeq 125$ GeV. The mixing angle α can be expressed in terms of λ_3 as

$$
\sin(2\alpha) \simeq \frac{2vv_{B-L}}{m_\phi^2 - m_h^2}\lambda_3 = \frac{vm_{Z'}}{m_\phi^2 - m_h^2}\frac{\lambda_3}{g_{B-L}},
\tag{12}
$$

where we have used Eq. (6) in the last equality.

In terms of h and ϕ, the scalar potential (5) is rewritten as

$$
\begin{aligned}
V &= \frac{1}{2}m_h^2 h^2 + \frac{1}{2}m_\phi^2\phi^2 + \frac{1}{6}C_{hhh}h^3 + \frac{1}{2}C_{hh\phi}h^2\phi \\
&\quad + \frac{1}{2}C_{h\phi\phi}h\phi^2 + \frac{1}{6}C_{\phi\phi\phi}\phi^3 + \cdots,
\end{aligned}
\tag{13}
$$

where the ellipsis denotes quartic terms that are irrelevant for our following analysis. The scalar trilinear couplings are given by

$$
C_{hhh} = 3\frac{m_h^2(v_{B-L}\cos^3\alpha - v\sin^3\alpha)}{vv_{B-L}},
\tag{14a}
$$

$$
C_{hh\phi} = \frac{\sin(2\alpha)(2m_h^2 + m_\phi^2)(v\sin\alpha + v_{B-L}\cos\alpha)}{2vv_{B-L}},
\tag{14b}
$$

$$
C_{h\phi\phi} = \frac{\sin(2\alpha)(m_h^2 + 2m_\phi^2)(v_{B-L}\sin\alpha - v\cos\alpha)}{2vv_{B-L}},
\tag{14c}
$$

$$
C_{\phi\phi\phi} = 3\frac{m_\phi^2(v\cos^3\alpha + v_{B-L}\sin^3\alpha)}{vv_{B-L}},
\tag{14d}
$$

where $C_{hh\phi}$ and $C_{h\phi\phi}$ are suppressed for the small mixing angle α.

Similarly, each Yukawa coupling of the SM fermions f and RH neutrinos ν_R with h and ϕ is suppressed due to the Higgs mixing with the following factor

$$
C_{hf} = \cos\alpha,
\tag{15a}
$$

$$
C_{\phi f} = \sin\alpha,
\tag{15b}
$$

$$
C_{h\nu_R} = -\sin\alpha,
\tag{15c}
$$

$$
C_{\phi\nu_R} = \cos\alpha,
\tag{15d}
$$

and the mixing suppression factors to the gauge couplings of the SM gauge bosons $V(W, Z, A)$ and Z' to h and ϕ are given by

$$
C_{hV} = \cos\alpha,
\tag{16a}
$$

$$
C_{\phi V} = \sin\alpha,
\tag{16b}
$$

$$C_{hZ'} = -\sin\alpha, \qquad (16c)$$

$$C_{\phi Z'} = \cos\alpha. \qquad (16d)$$

From the above equations, we can read the interactions of Z' and ν_R^i are affected by the Higgs mixing. We will see later that the mixing is essential for the production of the sterile neutrino DM in some cases.

2. Decays of scalars and range of Higgs mixing

Due to the Higgs mixing, decay rates of the SM-like Higgs boson into the SM particles are multiplied by $\cos^2\alpha$ in our model. In addition, if the mass of the singletlike scalar ϕ is smaller than one half of the SM-like Higgs boson mass, another decay mode $h \to \phi\phi$ is possible. Thus, the partial decay rates of h are given by

$$\Gamma_h(h \to \mathrm{SM}) = \cos^2\alpha\,\Gamma_{h_{\mathrm{SM}}}(h_{\mathrm{SM}} \to \mathrm{SM}), \qquad (17a)$$

$$\Gamma_h(h \to \phi\phi) = \frac{\sqrt{m_h^2 - 4m_\phi^2}}{16\pi m_h^2}|C_{h\phi\phi}|^2, \qquad (17b)$$

$$\Gamma_h(h \to Z'Z') = \frac{\sqrt{m_h^2 - 4m_{Z'}^2}}{32\pi m_h^2}\sin^2\alpha\,\frac{m_h^4 - 4m_h^2 m_{Z'}^2 + 12m_{Z'}^4}{v_{B-L}^2}, \qquad (17c)$$

$$\Gamma_h(h \to NN) = \sum_i \frac{1}{16\pi m_h}\left(1 - \frac{4m_{N_i}^2}{m_h^2}\right)^{3/2}\sin^2\alpha\,\frac{m_h^2 m_{N_i}^2}{v_{B-L}^2}, \qquad (17d)$$

where $h_{\mathrm{SM}} \to \mathrm{SM}$ stands for the decay processes of SM Higgs boson into all final states in the SM model and its decay rate is $\Gamma_{h_{\mathrm{SM}}}(h_{\mathrm{SM}} \to \mathrm{SM}) \simeq 4$ MeV. Here, m_{N_i} is the mass of sterile neutrinos and $m_{N_i} \simeq m_{\nu_R^i}$ for small active-sterile mixings.

The total decay rate Γ_h is given by the sum of Eqs. (17). For $m_\phi < m_h/2$, the current constraints on exotic decay of the SM Higgs boson as $\mathrm{Br}(h \to \mathrm{invisible}) \lesssim 19\%$ [35] can be recast as $\sin\alpha \lesssim 0.2$. For $m_\phi > m_h/2$, the obtained range $\alpha < \mathcal{O}(0.1)$ is also consistent with measurements in the LHC [36].

In the mass spectra of our interest, the singletlike scalar ϕ decays dominantly into pairs of the SM fermions through the Higgs mixing with the rate

$$\Gamma_\phi(\phi \to \mathrm{SM}) = \sin^2\alpha\,\Gamma_{h_{\mathrm{SM}}}(\phi \to \mathrm{SM}), \qquad (18)$$

where $\Gamma_{h_{\mathrm{SM}}}(\phi \to \mathrm{SM})$ expresses the decay rate of ϕ with the same SM interactions of h, and the scale of running parameters is taken at m_ϕ in the calculation. The following decay modes with partial decay rates

$$\Gamma_\phi(\phi \to hh) = \frac{\sqrt{m_\phi^2 - 4m_h^2}}{16\pi m_\phi^2}|C_{hh\phi}|^2, \qquad (19a)$$

$$\Gamma_\phi(\phi \to Z'Z') = \frac{\sqrt{m_\phi^2 - 4m_{Z'}^2}}{16\pi m_\phi^2}\cos^2\alpha \\ \times \frac{m_\phi^4 - 4m_\phi^2 m_{Z'}^2 + 12m_{Z'}^4}{v_{B-L}^2}, \qquad (19b)$$

$$\Gamma_\phi(\phi \to NN) = \sum_i \frac{1}{16\pi m_\phi}\left(1 - \frac{4m_{N_i}^2}{m_\phi^2}\right)^{3/2}\cos^2\alpha\,\frac{m_\phi^2 m_{N_i}^2}{v_{B-L}^2}, \qquad (19c)$$

can also open depending on the mass spectrum. These, however, are negligible compared with Eq. (18); $\Gamma_\phi(\phi \to hh)$ is due to $v_{B-L} \gg v$, and the others are also with the suppression by v_{B-L} unless we take $\alpha \to 0$. Therefore, we find typically $\Gamma_\phi \sim \sin^2\alpha\,\mathrm{MeV}$. Bounds on the Higgs mixing between a light scalar and the SM-like Higgs boson have been derived from the LEP experiments similarly [37], and the range $\alpha < \mathcal{O}(0.1)$ coincides with the bounds as well.

If the singletlike scalar is lighter than about a few GeV, the constraints from meson decays by the LHCb [38,39] and CHARM [40] are more stringent than ATLAS, CMS, and the LEP. In such a mass range, the bound $10^{-5} \lesssim \sin\alpha \lesssim 10^{-4}$ has been obtained [41] where the lower bound is set by demanding that the lifetime of ϕ must be shorter than $\mathcal{O}(0.1)$ seconds so as not to affect the BBN [42].

III. THE BOLTZMANN EQUATION

In this section we describe our Boltzmann equations to calculate the evolution and abundance of the sterile neutrino DM and Z' via freeze-in production. Here and hereafter the DM is denoted with N, which is a suitable one among the three sterile neutrinos. The Boltzmann equations for the number density of N and Z' are given by

$$\frac{dn_N}{dt} + 3Hn_N = \sum_{i,j}\langle\sigma v(ij \to NN)\rangle(n_i n_j - n_N^2) \\ + \sum_i \langle\Gamma(i \to NN)\rangle n_i, \qquad (20a)$$

$$\frac{dn_{Z'}}{dt} + 3Hn_{Z'} = \sum_{i,j}\langle\sigma v(ij \to Z'Z')\rangle(n_i n_j - n_{Z'}^2) \\ + \sum_i \langle\Gamma(i \to Z'Z')\rangle n_i \\ + \sum_{i,j,k}\langle\sigma v(Z'i \to jk)n_i\rangle(n_{Z'} - n_{Z'}^{\mathrm{eq}}) \\ - \sum_{i,j}\langle\Gamma(Z' \to ij)\rangle(n_{Z'} - n_{Z'}^{\mathrm{eq}}), \qquad (20b)$$

where i, j, and k are possible initial and final states in reactions, and n_i is the number density of i-particle. Note that N and Z' productions from the decays of intermediate particles produced on-pole in the first term are treated properly to avoid double-counting in Eqs. (20). The cosmic expansion rate H in the radiation-dominated (RD) universe is given by

$$H^2 \equiv \left(\frac{\dot{a}}{a}\right)^2 = \frac{1}{3M_P^2}\rho_r, \qquad (21)$$

$$\rho_r = \frac{\pi^2 g_*}{30}T^4, \qquad (22)$$

where a is the scale factor of the universe and dot denotes derivative with respect to the cosmic time t. The reduced Planck mass is $M_P \simeq 2.4 \times 10^{18}$ GeV, ρ_r is the energy density of radiation with the temperature T and g_* denotes the number of relativistic degrees of freedom.

A thermally averaged product of the scattering cross section and the relative velocity in Eqs. (20a) and (20b) are given by [43]

$$\langle \sigma v \rangle n_i n_j = \frac{T}{32\pi^4}\sum_{i,j}\int_{(m_i+m_j)^2}^{\infty}ds\,g_i g_j p_{ij}4E_i E_j \sigma v K_1\left(\frac{\sqrt{s}}{T}\right), \qquad (23)$$

and

$$4E_i E_j \sigma v \equiv \prod_f \int \frac{d^3 p_f}{(2\pi)^3}\frac{1}{2E_f}\overline{|\mathcal{M}|^2}(2\pi)^4$$

$$\times \delta^{(4)}\left(p_i + p_j - \sum p_f\right)$$

$$= \frac{1}{16\pi}\frac{2|q_f|}{\sqrt{s}}\int \overline{|\mathcal{M}|^2}d\cos\theta, \qquad (24)$$

$$2|q_f| = \sqrt{s - 4m_N^2}, \qquad (25)$$

$$p_{ij} \equiv \frac{\sqrt{s - (m_i + m_j)^2}\sqrt{s - (m_i - m_j)^2}}{2\sqrt{s}}, \qquad (26)$$

where i is an initial state with mass m_i, energy E_i, and internal degrees of freedom g_i. The center-of-mass energy squared is given by $s = (E_i + E_j)^2$ and three-momentum of a final-state particle is denoted by q_f. $K_i(z)$ is the modified Bessel function of the ith kind.

We consider the vanishing limit of the active-sterile mixings unless otherwise stated in the following analyses. This is because our purpose is to investigate the production of N dominantly through the g_{B-L} gauge interaction. For the very small g_{B-L} we are interested in, the first term in

right-hand side of Eq. (20b) representing the pair productions $ij \to Z'Z'$ is actually negligible compared with the other terms. This is because the cross sections for such pair productions are suppressed by g_{B-L}^4 while processes described in other terms are suppressed by only g_{B-L}^2.

The second terms in the right-hand side of Eqs. (20a) and (20b) represent the production by the decay of an i-particle, and

$$\langle\Gamma(i \to NN \text{ or } Z'Z')\rangle = \frac{K_1\left(\frac{m_i}{T}\right)}{K_2\left(\frac{m_i}{T}\right)}\Gamma(i \to NN \text{ or } Z'Z'), \qquad (27)$$

is the thermal averaged partial decay rate of the i-particle which is suppressed for a high temperature, $T \gg m_i$, by the time dilation.

The third term in right-hand side of Eq. (20b) principally denotes the processes of $f\bar{f} \leftrightarrow Z'\gamma$, $f\gamma \leftrightarrow fZ'$ and $\bar{f}\gamma \leftrightarrow \bar{f}Z'$. The thermal averaging of σvn is defined as

$$\langle\sigma v n_i\rangle n_{Z'}^{\text{eq}} \equiv \frac{T}{32\pi^4}\int_{(m_i+m_{Z'})^2}^{\infty}ds\,g_i g_{Z'}p_{iZ'}(4E_i E_{Z'}\sigma v)$$

$$\times K_1\left(\frac{\sqrt{s}}{T}\right), \qquad (28)$$

with

$$n_{Z'}^{\text{eq}} = \frac{T}{2\pi^2}g_{Z'}m_{Z'}^2 K_2\left(\frac{m_{Z'}}{T}\right), \qquad (29)$$

where the superscript "eq" stands for the equilibrium value. Those turn out to be actually negligible compared with the fourth term. This can be understood from the fact that the cross sections of those $\gamma - Z'$ scatterings are suppressed by $g_{B-L}^2\alpha_{\text{em}}$ with $\alpha_{\text{em}} = e^2/(4\pi)$, while the following fourth term is suppressed by only g_{B-L}^2.

The fourth term in Eqs. (20b) denotes the decay and inverse decay of Z'. The extra neutral gauge boson Z' decays into all fermions charged under the $U(1)_{B-L}$. The partial decay widths of Z' are given by

$$\Gamma_{Z'}(Z' \to f\bar{f}) = \sum_f \frac{g_{B-L}^2 q_{B-L}^2 N_c}{12\pi m_{Z'}^2}(2m_f^2 + m_{Z'}^2)$$

$$\times (m_{Z'}^2 - 4m_f^2)^{1/2}, \qquad (30a)$$

$$\Gamma_{Z'}(Z' \to NN) = \sum_i \frac{g_{B-L}^2}{24\pi m_{Z'}^2}(m_{Z'}^2 - 4m_{N_i}^2)^{3/2}, \qquad (30b)$$

where the number of color $N_c = 3$ is for quark final states. In this paper, we consider the situation where h and ϕ are enough heavier than Z'. Then, the total decay rate is given by the sum of those. The inverse decay is the most efficient process to thermalize Z' disregarded in previous studies. This is our new observation in this work. Because of this

efficient thermalization of Z', we find the new freeze-in scenario where the $Z'Z' \to NN$ is the dominant production mode for $m_{Z'} \gtrsim 1$ MeV. On the other hand, for $m_{Z'} \lesssim 1$ MeV, the magnitude of the $B - L$ gauge coupling g_{B-L} turns out to be smaller than $\mathcal{O}(10^{-12})$ to avoid the overproduction of light Z' as dark radiation.

IV. ABUNDANCE OF STERILE NEUTRINO DM

In this section we present the parameter region where cosmological constraints are satisfied and the observed DM abundance is explained with N. The following three mass spectra are considered. Dominant processes of the DM production depend on the spectra, and hence the obtained regions are different in the three spectra. Before we show the results in detail, we briefly summarize those as

(a) *Heavy gauge boson region $m_{Z'} > 2m_N$*: The DM N and Z' are not thermalized in this case. The Z' are dominantly produced on shell by its inverse decay. The DM is produced by the subsequent nonthermal decay $Z' \to NN$. By taking the free-streaming length constraints into account for $m_{Z'} \lesssim 100$ GeV, the allowed mass range of N turns out to be $m_N \gtrsim 1$ MeV and $g_{B-L} > 10^{-12}$.

(b) *Light gauge boson region $2m_N > m_{Z'} > 1$ MeV*: Z' is thermalized by its inverse decay. The DM is dominantly produced via pair annihilation $Z'Z' \to NN$. In this case, the DM abundance depends on the mass of ϕ due to the s-channel exchange of ϕ. Taking $m_N = 1$ GeV and 1 GeV $< m_\phi < 100$ GeV, the allowed region is found in $10^{-10} < g_{B-L} < 10^{-6}$ and 10^{-3} GeV $< m_{Z'} < 2$ GeV.

(c) *Very light gauge boson region $2m_N > 1$ MeV $> m_{Z'}$*: The $B - L$ gauge coupling must be $g_{B-L} \lesssim 10^{-12}$ to avoid the BBN and the CMB constraints. The DM must be dominantly produced from the scatterings of the SM particles and ϕ via ϕ/h s-channel exchange.

A. Heavy gauge boson region $m_{Z'} > 2m_N$

The freeze-in DM production by the mediation of the extra gauge boson can be effective for $m_{Z'} > 2m_N$. Under this mass spectrum, the production of N can be dominated by the nonthermal decay of Z'. Since not only N but also Z' cannot be thermalized, we need to simultaneously solve the Boltzmann Eqs. (20a) and (20b), which are rewritten as

$$\left(\frac{dx}{dt}\right)\frac{dY_N}{dx} = \langle\Gamma(Z' \to NN)\rangle Y_{Z'}, \tag{31a}$$

$$\left(\frac{dx}{dt}\right)\frac{dY_{Z'}}{dx} = \langle\Gamma(\phi \to Z'Z')\rangle Y_\phi$$
$$- \sum \langle\sigma v(Z'i \leftrightarrow jk)n_i\rangle(Y_{Z'} - Y_{Z'}^{\text{eq}})$$
$$- \sum \langle\Gamma(Z' \leftrightarrow ij)\rangle(Y_{Z'} - Y_{Z'}^{\text{eq}}), \tag{31b}$$
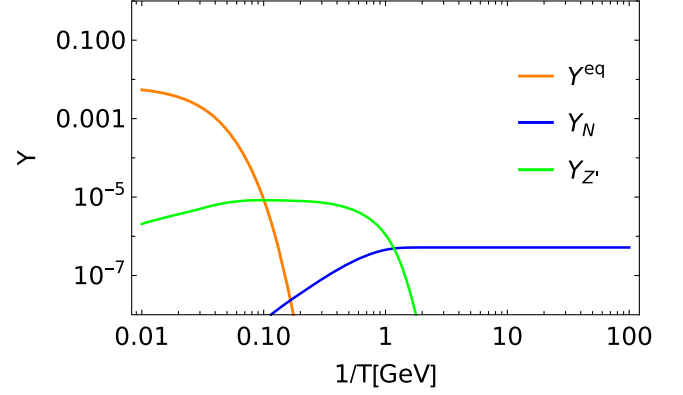

FIG. 1. Evolution of the yields of Z' and N for $m_{Z'} = 100$ GeV, $g_{B-L} = 5 \times 10^{-10}$, $m_N = 1$ MeV, $\alpha = 0$.

where $x \equiv M/T$ with M being a mass scale for the normalization is a dimensionless variable. The yield abundance $Y_i \equiv n_i/s$ is defined as the ratio of the number density to the entropy density

$$s = \frac{2\pi^2 g_{*S}}{45}T^3, \tag{32}$$

with g_{*S} being the total relativistic degrees of freedom for the entropy. Here, the pair production of N by scattering $ij \to NN$ is dominated by the resonant processes of s-channel Z' mediation from $f\bar{f}$ initial states. Since we have included the inverse decay of Z', $f\bar{f} \to Z'$, and the decay of Z' into NN, we have discarded the term for $f\bar{f} \to NN$ to avoid the double counting.

We show, in Fig. 1, the typical evolution of $Y_{Z'}$ and Y_N for $m_{Z'} = 100$ GeV, $g_{B-L} = 5 \times 10^{-10}$, $m_N = 1$ MeV, and $\alpha = 0$.[2] The orange curve is the thermal equilibrium yield value of the Z' boson. The blue and green solid curves represent values of $Y_{Z'}$ and Y_N, respectively. Here, we have confirmed that the $\gamma - Z'$ scatterings are negligible compared to the inverse decay of Z', as mentioned above. Once $Y_N(x \to \infty)$ is obtained, the present relic density is evaluated as

$$\Omega h^2 = \frac{m_N}{\rho_{\text{crit}}/s_0}Y_N, \tag{33}$$

where $(\rho_{\text{crit}}/s_0)^{-1} = 2.8 \times 10^8/\text{GeV}$ is given by the present entropy density s_0 and the critical density $\rho_{\text{crit}} = 3M_P^2 H_0^2$ with H_0 being the present Hubble parameter.

---

[2]This condition $\alpha = 0$ is taken to suppress scalar mediated processes and is not necessarily satisfied exactly. However, when α is sufficiently large, the scalar mediated processes easily dominate over the Z' mediated processes and it is reduced to the Higgs portal freeze-in Majorana DM model.

Since the DM N are produced by the decay of out-of-equilibrium Z', under the mass spectrum of $m_{Z'} \gg m_N$, N could be generated with a large momentum of about a half of the Z' mass. Such an energetic N can have a large free-streaming length and erase small scale structures. The resultant comoving free-streaming scale can be calculated as [44]

$$
\begin{aligned}
R_f &= \int_{t_{\text{dec}}}^{t_{\text{mre}}} \frac{v(t')}{a(t')} dt' \\
&\simeq \frac{1}{2a_{\text{mre}}H_{\text{mre}}} \frac{a_{\text{nr}}}{a_{\text{mre}}} \left(\log\left(1 + \frac{1}{\sqrt{1 + \left(\frac{a_{\text{nr}}}{a_{\text{mre}}}\right)^2}} \right) \right. \\
&\quad \left. - \log\left(1 - \frac{1}{\sqrt{1 + \left(\frac{a_{\text{nr}}}{a_{\text{mre}}}\right)^2}} \right) \right),
\end{aligned}
\tag{34}
$$

with the velocity v. The three-momentum of produced DM normalized by the mass

$$
\frac{p_N}{m_N} = u = \frac{v}{\sqrt{1 - v^2}},
\tag{35}
$$

whose initial value

$$
u(t_{\text{dec}}) = \frac{\sqrt{m_{Z'}^2 - 4m_N^2}}{2m_N},
\tag{36}
$$

is given at the time of the Z' decay, $t_{\text{dec}} = 1/\Gamma_{Z'}$, redshifts inversely proportional to the scale factor as $u \propto a(t_{\text{dec}})/a(t) = a_{\text{dec}}/a(t)$. The scale factor a_{nr} is one at the time t_{nr} when N becomes nonrelativistic, i.e., $u = 1$, which is evaluated as

$$
u(t_{\text{dec}}) \frac{a_{\text{dec}}}{a_{\text{nr}}} = 1.
\tag{37}
$$

At the time of the matter-radiation equality, t_{mre},

$$
\frac{a_0}{a_{\text{mre}}} = 1 + z_{\text{mre}} = \frac{\Omega_m h^2}{\Omega_r h^2},
\tag{38}
$$

$$
H_{\text{mre}} = \sqrt{2\Omega_m} H_0 (1 + z_{\text{mre}})^{3/2},
\tag{39}
$$

where $\Omega_{r(m)}$ is the density parameter of the radiation (matter), and a_0 and H_0 are the present scale factor and Hubble parameter, respectively. We find

$$
\frac{a_{\text{nr}}}{a_{\text{mre}}} = \frac{a_{\text{dec}}}{a_{\text{mre}}} u(t_{\text{dec}}) = \sqrt{\frac{t_{\text{mre}}}{t_{\text{dec}}}} u(t_{\text{dec}}),
\tag{40}
$$

from Eq. (37) and $a \propto \sqrt{t}$ in the RD universe. By substituting Eqs. (36), (38), (39), and (40) into Eq. (34),
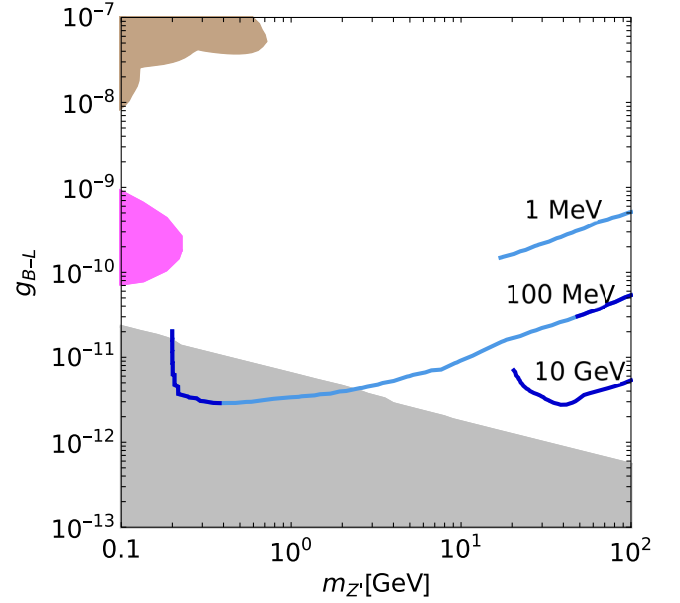

FIG. 2. Contours of $\Omega h^2 = 0.12$ for several values of m_N with bluish lines. The region with $1/\Gamma_{Z'} > 0.1$ second is shaded by gray, and regions excluded by the SN1987A constraint and beam dump experiments are colored magenta and brown, respectively.

we can evaluate the free-streaming length as $\lambda_{\text{fs}} = a_0 R_f$. While the non-negligible free-streaming length would be interesting from the viewpoint of small-scale problems in cold dark matter model, it should not be larger than sub-Mpc. The recent constraints on warm DM or the free-streaming scale have been reported in Ref. [45,46].

The contours of the observed DM density $\Omega h^2 = 0.12$ in Fig. 2 appear as blueish curves for $m_N = 1$ MeV, 100 MeV, and 10 GeV, from top to bottom, respectively. The dark and light blue curves correspond to $\lambda_{\text{fs}} < 0.01$ Mpc, and 0.01 Mpc $< \lambda_{\text{fs}} < 0.1$ Mpc, respectively. The left endpoint of the light blue curve for $M_N = 1$ MeV corresponds to $\lambda_{\text{fs}} = 0.1$ Mpc. From the line for $M_N = 100$ MeV, we can read that the free-streaming length is shortened not only for $m_{Z'} \gtrsim 2m_N$ but also for $m_{Z'} \gg m_N$. In the latter case, the Z' decay happens relatively early and thus there is enough time to be redshifted for the momentum of N. As long as we consider $m_{Z'} \lesssim 100$ GeV, the mass of the DM produced by this mechanism must be larger than about MeV to have a small enough free-streaming length. The region where the lifetime of the Z' boson is longer than 0.1 second is shaded in gray. It is ruled out because the decay of such long-lived abundant Z' bosons produces energetic particles and destroys the light elements synthesized by big bang nucleosynthesis. We employed the SN1987A constraint from Ref. [47] as a reference and the excluded region is colored magenta. For the constraint see also recent other discussions [48,49]. The region colored brown is excluded by
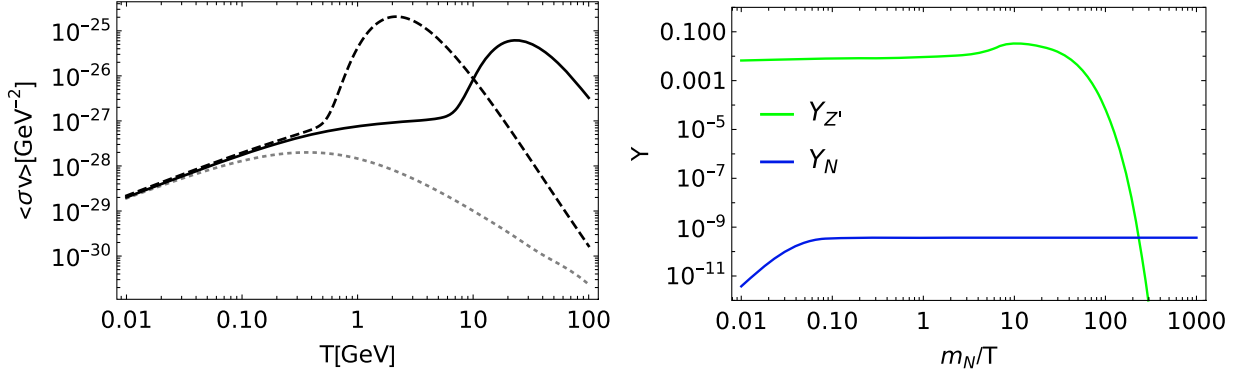
FIG. 3. Plots are made for $\alpha = 0$, $m_{Z'} = 0.1$ GeV, $g_{B-L} = 2 \times 10^{-8}$, $m_N = 1$ GeV. *Left*: $\langle \sigma v \rangle$ for $m_\phi = 1$ GeV (gray dotted), 10 GeV (black dashed), and 100 GeV (black solid). *Right*: Evolution of the yields of Z' (green curve) and N (blue curve) for $m_\phi = 100$ GeV. For this parameter set, $\Omega_N h^2 \simeq 0.1$ is reproduced.

electron and proton beam dump experiments ([50,51] and references therein).[3]

B. Light gauge boson region: $2m_N > m_{Z'} > 1$ MeV

Next, we consider the mass spectrum of $2m_N > m_{Z'} > 1$ MeV, in which the lower limit corresponds to the typical temperature of BBN. If we consider a smaller mass of Z' or larger coupling g_{B-L} than the parameter sets studied in Sec. IV A, the Z' gauge boson is fully thermalized by its decay and inverse decay described by the fourth terms in the right-hand side of Eq. (20b).

As a result, N is dominantly produced by the pair-production processes $Z'Z' \to NN$ via $t(u)$-channel N exchange processes and s-channel ϕ and h exchange processes. The remarkable feature is the m_ϕ dependence of the DM abundance. For $m_{Z'} < m_N$, the scattering cross section of this process grows with respect to s at lower energy than the mediator mass scale due to the longitudinal mode of Z'. In fact, the leading part of invariant amplitude squared, whose full expression is noted in Appendix, at a large $s > m_N^2 \gg m_{Z'}^2$ is

$$\int \sum |\mathcal{M}|^2 d\cos\theta \sim \frac{32 g_{B-L}^4}{m_{Z'}^4} \left(\frac{2m_N^4 s^2}{m_N^2(s - 4m_{Z'}^2) + m_{Z'}^4} - \frac{2m_N^2 s^3}{\Gamma_\phi^2 m_\phi^2 + (m_\phi^2 - s)^2} \right), \quad (41)$$

---

[3]The excluded regions by beam dump experiments and SN1987A have been derived under the assumption that Z' does not decay into RH neutrinos. Therefore, although Fig. 2 is presented for the $m_{Z'} > 2m_N$ case, the shaded area would not be exact. We, however, show them for reference purposes, because the excluded region is very far away from the parameter region of our interest and the viable parameter space of DM is unaffected. Since sterile neutrino N is also a very weakly-interacting light particle, N in addition to Z' would contribute the energy loss of supernovae. However, while the production cross section of Z' is as $\sigma \propto g_{B-L}^2$, that of N pair is $\sigma \propto g_{B-L}^8$ because the vertex of $f \to fNN$ is induced by the one loop diagram running N and Z' with f being SM particles. Thus, the latter is negligible compared with the former, for $g_{B-L} \ll 1$.

where θ is the scattering angle. The first term from the $t(u)$-channel N exchange processes grows linearly with respect to the center-of-mass energy s, as s becomes large. The second term from s-channel ϕ exchange processes becomes comparable for $s \gtrsim m_\phi^2$ and cancels with the first term at $s \gg m_\phi^2$. The m_ϕ dependence in the thermally averaged cross section for $m_N = 1$ GeV is shown in the left panel of Fig. 3. Each curve is for $m_\phi = 1$ GeV (gray dotted), 10 GeV (black dashed), and 100 GeV (black solid). The black dashed and solid curves for $m_\phi > m_N$ have a sharp peak at $T \sim m_\phi/5$ due to the resonance pole of ϕ and decrease at the high temperature region $T > \mathcal{O}(m_\phi)$. It should be emphasized here that the DM production takes place most effectively at not $T \sim m_N$ but $T \sim m_\phi/5$, unlike most freeze-in scenarios with renormalizable couplings. Hence, the result is sensitive to the mass of mediator m_ϕ.

This characteristic dependence of m_ϕ can be seen concretely in an example of the evolution of $Y_{Z'}$ and Y_N for $m_N = 1$ GeV, $m_\phi = 100$ GeV, $m_{Z'} = 0.1$ GeV, $g_{B-L} = 2 \times 10^{-8}$, $\alpha = 0$ presented in right panel of Fig. 3. The blue and green curves represent values of Y_N and $Y_{Z'}$, respectively. The Z' boson is thermalized and its yield follows the thermal value. The slight increase of $Y_{Z'}$ around $m_N/T \sim 10$ is due to the change of g_* at the quark hadron transition. We can see that N is gradually generated until the temperature becomes as low as $\sim m_\phi/5$ not the DM mass m_N. The energy density of Z' decreases due to the Boltzmann suppression. Thus, the energy density of Z' gets negligible by the onset of the BBN.

The contours of $\Omega h^2 = 0.12$ in this mass spectrum are shown in Fig. 4. The colored, excluded regions are the same as Fig. 2. The curves shift to the right or left when we increase or decrease m_N. We also note that parameters to reproduce the observed DM abundance interestingly lie in the reach of future experiments for long-lived particle search or beam dump experiments.

C. Very light gauge boson region: $2m_N > 1$ MeV $> m_{Z'}$

Finally, we consider the mass spectrum of $2m_N > 1$ MeV $> m_{Z'}$. If such a light Z' boson is thermalized by
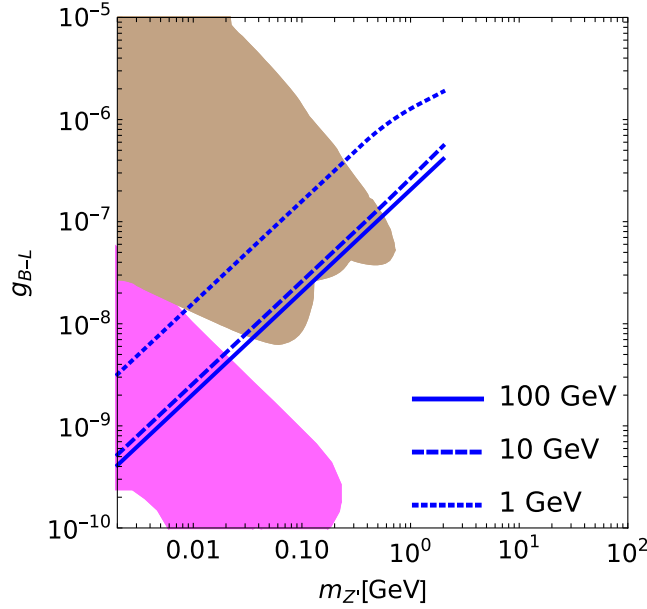
FIG. 4. Same as Fig. 2, but for $2m_N > m_{Z'} > 1$ MeV. Contours of $\Omega h^2 = 0.12$ with $m_N = 1$ GeV are shown by blue dotted, dashed, and solid curves for $m_\phi = 1, 10, 100$ GeV, respectively.

its inverse decay, the contribution of Z' to the energy density of relativistic degrees of freedom at the BBN conflicts with the observation. To avoid this, the gauge coupling constant must be much smaller than about 10^{-10}. The smallness of the coupling makes all processes for sterile neutrino production via g_{B-L} gauge interaction negligible. However, $f\bar{f} \to NN$, $W^+W^-(ZZ) \to NN$ and $hh(h\phi, \phi\phi) \to NN$ of all the s-channel scalar (h or ϕ) exchanges are relevant processes to produce the DM N. Those processes get effective at the electroweak and $B - L$ broken vacuum, and thus only $b\bar{b}$ and $\tau\bar{\tau}$ initial states are dominant, $\phi\phi$ initial state could be non-negligible for some parameter sets, and the other initial states are negligible.

Since the evolution of abundance of N and Z' are independent in this case, two Boltzmann equations (20a) and (20b) are decoupled. We can solve both individually. First, let us see the evolution of the abundance of the gauge boson Z',

$$\frac{dn_{Z'}}{dt} + 3Hn_{Z'} = -\sum \langle \Gamma(Z' \leftrightarrow ij) \rangle (n_{Z'} - n_{Z'}^{\text{eq}}), \quad (42)$$

where we omit negligible inverse processes and negligible terms $\sigma v(ij \leftrightarrow Z'Z')$, $\Gamma(i \leftrightarrow Z'Z')$, and the $\gamma - Z'$ scattering. The term in the right-hand side is the decay and the inverse decay of Z'. The final abundance is determined by g_{B-L}, because the magnitude of the rate is proportional to g_{B-L}^2. In Fig. 5, the evolution of the energy density of Z' for $g_{B-L} = 5 \times 10^{-12}$ is shown and compared with that of one generation of neutrino. Because of the very long lifetime of Z', the constraint from CMB is much more stringent than
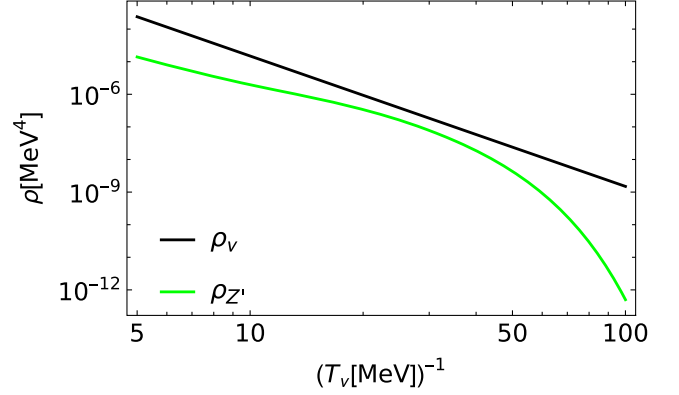

FIG. 5. The evolution of the energy density of Z' (green) and one generation of neutrino (black) for $g_{B-L} = 5 \times 10^{-12}$, $m_{Z'} = 0.3$ MeV, $m_N = 1$ GeV, and $m_\phi = 500$ GeV.

that from the BBN. As seen in Fig. 5, even if the abundance of Z' is sufficiently small at the time of the BBN $T_\nu \sim 1$ MeV, the energy fraction starts to increase for $T \lesssim m_{Z'}$ because the energy density decreases as a^{-3} after Z' becomes nonrelativistic. Thus, the extra radiation generated by Z' decay could be significant at the recombination epoch and affects the temperature anisotropy of CMB unless the energy density of Z' is small sufficiently at the BBN era.

While the evolution of the energy density of Z' can be followed as above, the abundance of Z' can be easily and directly estimated by the following single integration expression

$$Y_{Z'} = \int_{T_0}^{T_R} \frac{\sum \langle \Gamma(Z' \leftrightarrow ij) \rangle n_i n_j}{sTH} dT$$

$$= \frac{135\sqrt{10}M_P}{2\pi^3} \int_{T_0}^{T_R} \frac{dT}{g_{*S}\sqrt{g_*}T^6} \sum_{i,j} \langle \Gamma(Z' \leftrightarrow ij) \rangle n_{Z'}^{\text{eq}},$$

(43)

where T_0 is a low temperature before the decay of Z'. The Z' decays into LH neutrino pairs at $t = 1/\Gamma_{Z'}$. By comparing the energy density of neutrino of one species

$$\rho_\nu = g_\nu \frac{7}{8}\frac{\pi^2}{30}T_\nu^4, \quad (44)$$

where $g_\nu = 2$ is the internal degrees of freedom of neutrinos and T_ν is the temperature of neutrinos, the energy density of decay products from Z' can be parametrized as

$$\Delta N_{\text{eff}} \equiv \left.\frac{\rho_{Z'}}{\rho_\nu}\right|_{t=1/\Gamma_{Z'}}. \quad (45)$$

Similarly, by integrating Eq. (20a) from a low temperature T_0 to the reheating temperature after inflation T_R as
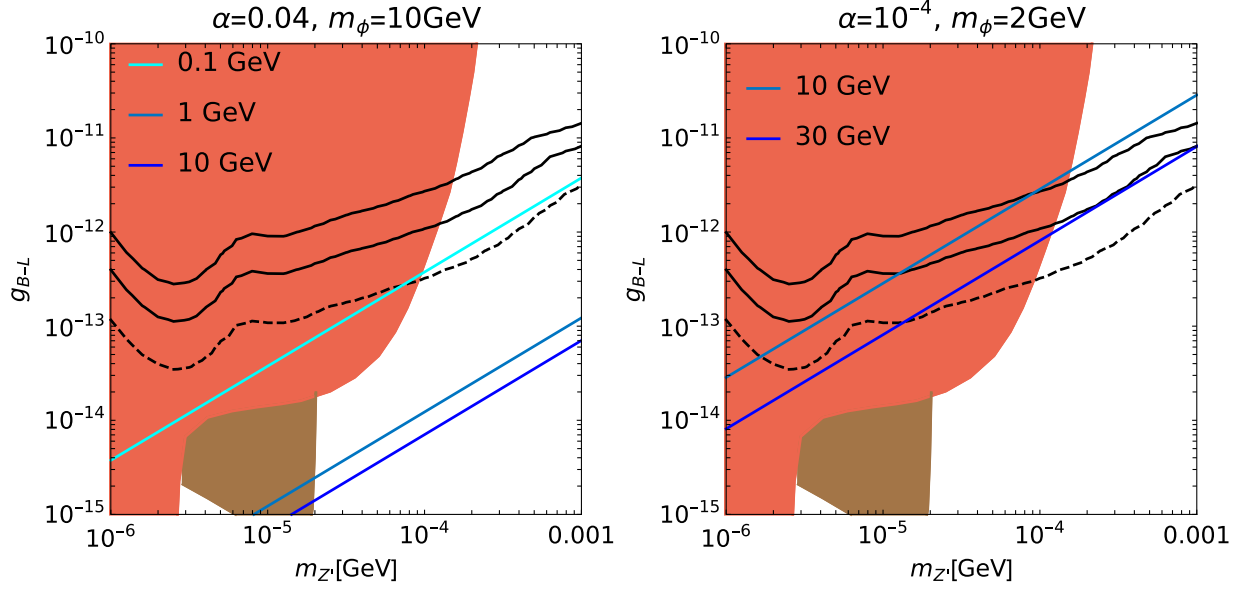
FIG. 6. Contours of $\Omega h^2 = 0.12$ and ΔN_{eff} presented with the parameter region excluded by the constraints from the horizontal branch star and red giant stars. The contours of $\Omega h^2 = 0.12$ are drawn with bluish lines for some m_N in key. The contours with black (solid, solid and dashed) curves are for $\Delta N_{\text{eff}} = 0.5$, 0.2, and 0.06 from top to bottom, respectively. *Left*: Contours for $\alpha = 0.04$, and $m_\phi = 10$ GeV. *Right*: Contours for $\alpha = 10^{-4}$, and $m_\phi = 2$ GeV.

$$Y_N = \int_{T_0}^{T_R} \frac{\langle \sigma v(ij \to NN) \rangle n_i n_j}{sTH} dT$$

$$= \frac{135\sqrt{10}M_P}{64\pi^7} \int_{T_0}^{T_R} \frac{dT}{g_{*S}\sqrt{g_*}T^5}$$

$$\times \sum_{i,j} \int_{(m_i+m_j)^2}^{\infty} ds g_i g_j p_{ij} 4E_i E_j \sigma v K_1\left(\frac{\sqrt{s}}{T}\right), \quad (46)$$

in the second equality, we have used Eqs. (21) and (22). In this framework, there are five free parameters associated with the production of DM N; $g_{B-L}, m_{Z'}, m_N, m_\phi$, and α. Although Ωh^2 seems to be dependent on all the five parameters, it practically depends on only three of $g_{B-L}\sin(2\alpha)/m_{Z'}, m_\phi$, and m_N. We can find a simple scaling of the resultant abundance as

$$\Omega h^2 \propto \left(\frac{g_{B-L}\sin(2\alpha)}{m_{Z'}}\right)^2, \quad (47)$$

because the coupling vertex appears only in this combination for the Higgs portal main processes. As we discussed in Sec. II, the Higgs mixing is constrained as $\alpha \lesssim 0.1$ for $m_\phi \gtrsim 10$ GeV and $\alpha \lesssim 10^{-4}$ for $m_\phi \lesssim$ several GeV.

In Fig. 6 the contours of $\Omega h^2 = 0.12$ are shown with bluish curves for some m_N and for two sets of α and m_ϕ. Two black solid and one black dashed curves are contours of $\Delta N_{\text{eff}} = 0.5$, 0.2, and 0.06 from top to bottom, respectively. We note that extra relativistic degrees of freedom with $0.2 \lesssim \Delta N_{\text{eff}} \lesssim 0.5$ would be favored to relax the

so-called Hubble tension [52–54] and that $\Delta N_{\text{eff}} = 0.06$ is the expected reach of the future experiment CMB-S4 [55]. The excluded region by the horizontal branch star and the red giant star constraints are shaded with orange and brown, respectively [56,57]. In the left panel, three lines of $\Omega_N h^2 \simeq 0.12$ are shown for $m_N = 0.1$, 1, and 10 GeV. The uneven intervals are due to the change of available modes. Namely, for a smaller m_N, the pair-production mode with heavy SM fermion initial states are suppressed at $T \sim m_N$. The right plot is an example with smaller m_ϕ and α. In this case, the larger $m_N > \mathcal{O}(10)$ GeV is required to reproduce the desired DM abundance, because the production cross section is strongly suppressed by the tiny mixing α.

V. IMPLICATION OF STERILE NEUTRINO DM DETECTION

We have considered sterile neutrino DM whose mass is larger than MeV. The visible decay modes include $N \to \nu\gamma$, three body decay $N \to \nu f\bar{f}$ through off-shell $W^\pm$ and Z, and even hadronic mode.[4] While the usual keV scale sterile neutrino DM is searched for with x-ray lines induced by its radiative decay [60], the DM argued in this paper can be also probed by seeking other modes, such as the decay into e^-e^+ and the continuous spectrum of gamma rays from hadrons.

All the decays are induced by the SM processes through the active-sterile mixing for $m_N < m_{Z'}$. On the other hand,

---

[4]For formulas of those decay rates, see for instance Refs. [58,59].

for $m_N > m_{Z'}$, a new decay mode $N \to \nu Z'$ is additionally possible, and thus signals to search for N are decided by the decay modes of Z' depending on $m_{Z'}$. In the very light gauge boson region, Z' can decay into only neutrinos, while decaying modes into other fermions opens as the mass increases.

Therefore, some of the decay rates depend on whether Z' is heavier than N or not, for example, the rate of $N \to e^- e^+ \nu$. Since $N \to \nu Z'$ is a tree-level process, the constraint on the active-sterile mixing may be more stringent than that from x-ray observations, especially for $m_N > m_{Z'}$ cases. The detailed study is beyond the scope of this paper, and we will evaluate this issue elsewhere.

VI. CONCLUSION

We have evaluated the freeze-in production of $U(1)_{B-L}$ gauge interacting sterile neutrino DM by taking into account processes overlooked in the literature; principally the inverse decay of Z' and the longitudinal mode effect in $Z'Z' \to NN$ scattering. We have found that the inverse decay of Z' indeed gives a non-negligible contribution to the production of Z'.

For $m_{Z'} > 2m_N$ cases, the final value of $\Omega_N h^2$ agrees with the previous estimation. Our finding for this mass spectrum case is that the constraint from the free-streaming length is more stringent than that has been thought. As the result, the mass of sterile neutrino DM under this mass spectrum must be larger than about one MeV as long as we assume $m_{Z'} \lesssim 100$ GeV.

For the other spectrum $m_{Z'} < 2m_N$, the gauge coupling $g_{B-L} = \mathcal{O}(10^{-6})$ independent from the $m_{Z'}$ has been regarded as the viable parameter region to reproduce the desired DM abundance. We, however, have found that this is not correct. Since Z' is lighter than N, when N is produced by $Z'Z' \to NN$, this cross section is enhanced by small $m_{Z'}^2$ and increases with respect to the energy until $s \sim m_\phi^2$, due to the longitudinal mode of Z'. Thus, the resultant DM abundance depends on $m_{Z'}$ and m_ϕ. In addition, for such a large coupling of $g_{B-L} \sim 10^{-6}$, Z' can be thermalized and gives $\Delta N_{\text{eff}} \sim 1$ at the BBN epoch for $m_{Z'} \lesssim 1$ MeV. Moreover, CMB gives a more stringent constraint on the gauge coupling as $g_{B-L} \lesssim 10^{-12}$ than BBN, because the energy density of Z' decreases slower than the background radiation after it becomes nonrelativistic. Thus, for $2m_N > 1$ MeV $> m_{Z'}$, the freeze-in production by the Z' mediation is not available and the DM in this parameter region can be produced only by scalar portal scatterings.

Having the parameter space of consistent sterile neutrino DM mentioned above, the viable parameters for $m_{Z'} > 2m_N$ lie far beyond the reach of the near future experiments of long-lived particle searches as shown in Fig. 2, while a large interesting parameter space in the spectrum of 1 MeV $< m_{Z'} < 2m_N$ is already constrained partially by the current experimental limits and will be probed more by the experiments in future. The case of the spectrum with $m_{Z'} < 1$ MeV $< 2m_N$ will be examined by future measurements of N_{eff}.

APPENDIX A: AMPLITUDE OF THE STERILE NEUTRINO PAIR-PRODUCTION PROCESSES

We give explicit formulas of the invariant amplitude squared.

1. $f(p_1)\bar{f}(p_2) \to N(q_1)N(q_2)$

$$\overline{|\mathcal{M}|^2} d\cos\theta = \frac{m_f^2 m_N^2 N_c \sin^2(2\alpha)(s - 4m_f^2)(s - 4m_N^2)}{2v^2 v_{B-L}^2}$$
$$\times \left| \frac{-1}{s - m_h^2 - i\Gamma_h m_h} + \frac{1}{s - m_\phi^2 - im_\phi\Gamma_\phi} \right|^2, \tag{A1}$$

$$4E_i E_j \sigma v(ij \to) = \frac{1}{16\pi} \sqrt{\frac{s - 4m_N^2}{s}} \overline{|\mathcal{M}|^2} d\cos\theta, \tag{A2}$$

$$p_{ij} = \frac{\sqrt{s - 4m_f^2}}{2}. \tag{A3}$$

2. $W(p_1)W(p_2) \to N(q_1)N(q_2)$

$$\overline{|\mathcal{M}|^2} d\cos\theta = \frac{g_2^2 m_N^2 \sin^2(2\alpha)(s - 4m_N^2)(-4m_N^2(2m_W^2 + s) + 4m_N^4 + 16m_W^4 + s^2)}{36m_W^2 v_{B-L}^2}$$
$$\times \left| \frac{-1}{s - m_h^2 - i\Gamma_h m_h} + \frac{1}{s - m_\phi^2 - im_\phi\Gamma_\phi} \right|^2, \tag{A4}$$

$$4E_i E_j \sigma v(ij \to) = \frac{1}{16\pi} \sqrt{\frac{s - 4m_N^2}{s}} \int \overline{|\mathcal{M}|^2} d\cos\theta, \tag{A5}$$

$$p_{ij} = \frac{\sqrt{s - 4m_W^2}}{2}. \tag{A6}$$

3. $Z(p_1)Z(p_2) \to N(q_1)N(q_2)$

$$\overline{|\mathcal{M}|^2} d\cos\theta = \frac{g_2^2 m_N^2 \sin^2(2\alpha)(s - 4m_N^2)(-4m_N^2(2m_Z^2 + s) + 4m_N^4 + 16m_Z^4 + s^2)}{36 m_Z^2 c_W^2 v_{B-L}^2}$$

$$\times \left| \frac{-1}{s - m_h^2 - i\Gamma_h m_h} + \frac{1}{s - m_\phi^2 - im_\phi \Gamma_\phi} \right|^2, \tag{A7}$$

$$4E_i E_j \sigma v(ij \to) = \frac{1}{16\pi} \sqrt{\frac{s - 4m_N^2}{s}} \int \overline{|\mathcal{M}|^2} d\cos\theta, \tag{A8}$$

$$p_{ij} = \frac{\sqrt{s - 4m_Z^2}}{2}. \tag{A9}$$

4. $(h,\phi)(p_1)(h,\phi)(p_2) \to N(p_1)N(p_2)$

$$i\mathcal{M} = -\frac{im_N \bar{u}(p_1, m_N) v(p_2, m_N)}{v_{B-L}} \left(\frac{C_h \sin\alpha}{(q_1 + q_2)^2 - m_h^2 + i\Gamma_h m_h} + \frac{C_\phi \cos\alpha}{(q_1 + q_2)^2 - m_\phi^2 + im_\phi \Gamma_\phi} \right), \tag{A10}$$

where we have omitted $t(u)$-channel N exchange contributions because those are suppressed by m_N^2/v_{B-L}^2 and are thus negligible.

$$\overline{|\mathcal{M}_s|^2} d\cos\theta = \frac{4m_N^2(s - 4m_N^2)}{v_{B-L}^2} \left| \frac{C_h \sin\alpha}{s - m_h^2 + i\Gamma_h m_h} + \frac{C_\phi \cos\alpha}{s - m_\phi^2 + im_\phi \Gamma_\phi} \right|^2,$$

$$(C_h, C_\phi) = (C_{h\phi\phi}, C_{\phi\phi\phi}) \quad \text{for } (\phi, \phi),$$
$$(C_{hh\phi}, C_{h\phi\phi}) \quad \text{for } (h, \phi),$$
$$(C_{hhh}, C_{hh\phi}) \quad \text{for } (h, h), \tag{A11}$$

$$4E_i E_j \sigma v(ij \to) = \frac{1}{16\pi} \sqrt{\frac{s - 4m_N^2}{s}} \int \overline{|\mathcal{M}|^2} d\cos\theta, \tag{A12}$$

$$p_{ij} = \frac{1}{2} \sqrt{\frac{(s - (m_{\phi_i} - m_{\phi_j})^2)(s - (m_{\phi_i} + m_{\phi_j})^2)}{s}}. \tag{A13}$$

$$5. \; Z'(q_1)Z'(q_2) \rightarrow N(p_1)N(p_2)$$

$$\int \sum |\mathcal{M}|^2 d\cos\theta = \frac{32 g_{B-L}^4}{m_{Z'}^4} \left(\frac{4m_N^2(m_\phi^2 - s)(-2m_{Z'}^2 s + 4m_{Z'}^4 + s^2)}{\Gamma_\phi^2 m_\phi^2 + (m_\phi^2 - s)^2} - \frac{2m_N^2(4m_N^2 - s)(-4m_{Z'}^2 s + 12m_{Z'}^4 + s^2)}{\Gamma_\phi^2 m_\phi^2 + (m_\phi^2 - s)^2} \right.$$

$$\left. + \frac{2m_N^4(-8m_{Z'}^2 s + 8m_{Z'}^4 + s^2) + m_N^2 m_{Z'}^4(4m_{Z'}^2 + s) - 2m_{Z'}^8}{m_N^2(s - 4m_{Z'}^2) + m_{Z'}^4} \right)$$

$$+ \frac{32 g_{B-L}^4}{m_{Z'}^4 \sqrt{s - 4m_N^2}\sqrt{s - 4m_{Z'}^2}} \left(\frac{8m_N^2(s - m_\phi^2)(m_N^2(-4m_{Z'}^2 s + 8m_{Z'}^4 + s^2) - 2m_{Z'}^6)}{\Gamma_\phi^2 m_\phi^2 + (m_\phi^2 - s)^2} \right.$$

$$\left. - \frac{4m_N^4 s(s - 4m_{Z'}^2) + 4m_N^2 m_{Z'}^2(4m_{Z'}^2 - s)(m_{Z'}^2 + s) - m_{Z'}^4(4m_{Z'}^4 + s^2)}{s - 2m_{Z'}^2} \right)$$

$$\times \log\left(\frac{s - 2m_{Z'}^2 + \sqrt{s - 4m_N^2}\sqrt{s - 4m_{Z'}^2}}{s - 2m_{Z'}^2 - \sqrt{s - 4m_N^2}\sqrt{s - 4m_{Z'}^2}} \right), \tag{A14}$$

$$4E_i E_j \sigma v(ij \rightarrow) = \frac{1}{16\pi}\sqrt{\frac{s - 4m_N^2}{s}}\int \overline{|\mathcal{M}|^2} d\cos\theta, \tag{A15}$$

$$p_{ij} = \frac{\sqrt{s - 4m_{Z'}^2}}{2}. \tag{A16}$$

APPENDIX B: AMPLITUDE OF THE $\gamma - Z'$ SCATTERING PROCESSES

We give explicit formulas of the invariant amplitude squared.

$$1. \; Z'(q_1)\gamma(q_2) \rightarrow f(p_1)\bar{f}(p_2)$$

$$\int \sum |\mathcal{M}|^2 d\cos\theta = (g_{B-L} q_{Xf} e q_f)^2 \frac{32}{(s - m_{Z'}^2)^2} \left(\frac{\sqrt{s}(4m_f^2(s - m_{Z'}^2) - 8m_f^4 + m_{Z'}^4 + s^2)}{\sqrt{s - 4m_f^2}} \log\left(\frac{\sqrt{s} + \sqrt{s - 4m_f^2}}{\sqrt{s} - \sqrt{s - 4m_f^2}} \right) \right.$$

$$\left. - s(4m_f^2 + s) - m_{Z'}^4 \right), \tag{B1}$$

where the IR divergence at $s = m_{Z'}^2$ is due to the on-shell $t(u)$-channel mediator and can be regulated by introducing thermal photon mass [61].

$$4E_i E_j \sigma v(ij \rightarrow) = \frac{1}{16\pi}\sqrt{\frac{s - 4m_f^2}{s}}\int \overline{|\mathcal{M}|^2} d\cos\theta, \tag{B2}$$

$$p_{ij} = \frac{1}{2}\frac{s - m_{Z'}^2}{\sqrt{s}}. \tag{B3}$$

2. $Z'(q_1)f(q_2) \to \gamma(p_1)f(p_2)$

$$\int \sum |\mathcal{M}|^2 d\cos\theta = \frac{8(g_{B-L}q_{Xf}eq_f)^2}{s(m_f^2 - s)^2} \left(-m_f^4(m_{Z'}^2 + s) + m_f^2 s(2m_{Z'}^2 + 15s) + m_f^6 + s^2(7m_{Z'}^2 + s) \right.$$

$$+ \frac{2s^2(2m_f^2(m_{Z'}^2 - 3s) - 3m_f^4 - 2m_{Z'}^2 s + 2m_{Z'}^4 + s^2)}{\sqrt{(s - (m_f - m_{Z'})^2)(s - (m_f + m_{Z'})^2)}}$$

$$\left. \times \log\left(\frac{m_f^2 - m_{Z'}^2 + s + \sqrt{(s - (m_f - m_{Z'})^2)(s - (m_f + m_{Z'})^2)}}{m_f^2 - m_{Z'}^2 + s - \sqrt{(s - (m_f - m_{Z'})^2)(s - (m_f + m_{Z'})^2)}} \right) \right), \tag{B4}$$

$$4E_i E_j \sigma v(ij \to) = \frac{1}{16\pi} \sqrt{\frac{s - m_f^2}{s}} \int \overline{|\mathcal{M}|^2} d\cos\theta, \tag{B5}$$

$$p_{ij} = \frac{1}{2} \sqrt{\frac{(s - (m_f - m_{Z'})^2)(s - (m_f + m_{Z'})^2)}{s}}. \tag{B6}$$

3. $Z'(q_1)\bar{f}(q_2) \to \gamma(p_1)\bar{f}(p_2)$

It is same as for $Z'(q_1)f(q_2) \to \gamma(p_1)f(p_2)$.

---

[1] P. Minkowski, Phys. Lett. **67B**, 421 (1977).
[2] T. Yanagida, Conf. Proc. C **7902131**, 95 (1979).
[3] M. Gell-Mann, P. Ramond, and R. Slansky, Conf. Proc. C **790927**, 315 (1979).
[4] R. N. Mohapatra and G. Senjanovic, Phys. Rev. Lett. **44**, 912 (1980).
[5] A. Dolgov and S. Hansen, Astropart. Phys. **16**, 339 (2002).
[6] M. Drewes *et al.*, J. Cosmol. Astropart. Phys. 01 (2017) 025.
[7] A. Boyarsky, M. Drewes, T. Lasserre, S. Mertens, and O. Ruchayskiy, Prog. Part. Nucl. Phys. **104**, 1 (2019).
[8] T. Asaka, S. Blanchet, and M. Shaposhnikov, Phys. Lett. B **631**, 151 (2005).
[9] T. Asaka and M. Shaposhnikov, Phys. Lett. B **620**, 17 (2005).
[10] A. Davidson, Phys. Rev. D **20**, 776 (1979).
[11] R. N. Mohapatra and R. Marshak, Phys. Rev. Lett. **44**, 1316 (1980); **44**, 1643(E) (1980).
[12] R. Marshak and R. N. Mohapatra, Phys. Lett. **91B**, 222 (1980).
[13] S. Dodelson and L. M. Widrow, Phys. Rev. Lett. **72**, 17 (1994).
[14] A. Boyarsky, A. Neronov, O. Ruchayskiy, and M. Shaposhnikov, Mon. Not. R. Astron. Soc. **370**, 213 (2006).
[15] A. Boyarsky, A. Neronov, O. Ruchayskiy, M. Shaposhnikov, and I. Tkachev, Phys. Rev. Lett. **97**, 261302 (2006).
[16] A. Boyarsky, J. Nevalainen, and O. Ruchayskiy, Astron. Astrophys. **471**, 51 (2007).
[17] A. Boyarsky, D. Iakubovskyi, O. Ruchayskiy, and V. Savchenko, Mon. Not. R. Astron. Soc. **387**, 1361 (2008).
[18] H. Yuksel, J. F. Beacom, and C. R. Watson, Phys. Rev. Lett. **101**, 121301 (2008).
[19] S. Khalil and O. Seto, J. Cosmol. Astropart. Phys. 10 (2008) 024.
[20] K. Kaneta, Z. Kang, and H.-S. Lee, J. High Energy Phys. 02 (2017) 031.
[21] A. Biswas and A. Gupta, J. Cosmol. Astropart. Phys. 09 (2016) 044; 05 (2017) A01.
[22] O. Seto and T. Shimomura, Phys. Lett. B **811**, 135880 (2020).
[23] V. De Romeri, D. Karamitros, O. Lebedev, and T. Toma, J. High Energy Phys. 10 (2020) 137.
[24] M. Lucente, arXiv:2103.03253.
[25] G. Bélanger, S. Khan, R. Padhan, M. Mitra, and S. Shil, Phys. Rev. D **104**, 055047 (2021).
[26] L. J. Hall, K. Jedamzik, J. March-Russell, and S. M. West, J. High Energy Phys. 03 (2010) 80.

[27] H. Baer, K.-Y. Choi, J. E. Kim, and L. Roszkowski, Phys. Rep. **555,** 1 (2015).

[28] B. Shakya, Mod. Phys. Lett. **31A,** 1630005 (2016).

[29] P. Fileviez Pérez, C. Murgui, and A. D. Plascencia, Phys. Rev. D **100,** 035041 (2019).

[30] S. Heeba and F. Kahlhoefer, Phys. Rev. D **101,** 035043 (2020).

[31] N. Okada, S. Okada, and Q. Shafi, Phys. Lett. B **810,** 135845 (2020).

[32] H. Okada, Y. Orikasa, and Y. Shoji, J. Cosmol. Astropart. Phys. 07 (2021) 006.

[33] S. Iwamoto, K. Seller, and Z. Trócsányi, J. Cosmol. Astropart. Phys. 01 (2022) 035.

[34] A. Caputo, A. J. Millar, C. A. J. O'Hare, and E. Vitagliano, Phys. Rev. D **104,** 095029 (2021).

[35] P. A. Zyla et al. (Particle Data Group), Prog. Theor. Exp. Phys. **2020,** 083C01 (2020).

[36] G. Aad et al. (ATLAS Collaboration), Phys. Rev. D **101,** 012002 (2020).

[37] R. Barate et al. (LEP Working Group for Higgs boson searches, ALEPH, DELPHI, L3, and OPAL Collaborations), Phys. Lett. B **565,** 61 (2003).

[38] R. Aaij et al. (LHCb Collaboration), Phys. Rev. Lett. **115,** 161802 (2015).

[39] R. Aaij et al. (LHCb Collaboration), Phys. Rev. D **95,** 071101 (2017).

[40] F. Bergsma et al. (CHARM Collaboration), Phys. Lett. **157B,** 458 (1985).

[41] M. W. Winkler, Phys. Rev. D **99,** 015018 (2019).

[42] A. Fradette and M. Pospelov, Phys. Rev. D **96,** 075033 (2017).

[43] P. Gondolo and G. Gelmini, Nucl. Phys. **B360,** 145 (1991).

[44] E. W. Kolb and M. S. Turner, The Early Universe, Frontiers in Physics Vol. 69 (Addison-Wesley, Reading, MA, 1990), ISBN 978-0-201-116038.

[45] V. Iršič et al., Phys. Rev. D **96,** 023522 (2017).

[46] E. O. Nadler et al. (DES Collaboration), Phys. Rev. Lett. **126,** 091101 (2021).

[47] D. Croon, G. Elor, R. K. Leane, and S. D. McDermott, J. High Energy Phys. 01 (2021) 107.

[48] C. S. Shin and S. Yun, J. High Energy Phys. 02 (2022) 133.

[49] A. Caputo, G. Raffelt, and E. Vitagliano, J. Cosmol. Astropart. Phys. 08 (2022) 045.

[50] J. L. Feng et al., arXiv:2203.05090.

[51] K. Asai, A. Das, J. Li, T. Nomura, and O. Seto, arXiv:2206.12676.

[52] N. Aghanim et al. (Planck Collaboration), Astron. Astrophys. **641,** A6 (2020); **652,** C4 (2021).

[53] O. Seto and Y. Toda, Phys. Rev. D **103,** 123501 (2021).

[54] O. Seto and Y. Toda, Phys. Rev. D **104,** 063019 (2021).

[55] K. Abazajian et al., arXiv:1907.04473.

[56] J. Redondo and G. Raffelt, J. Cosmol. Astropart. Phys. 08 (2013) 034.

[57] J. Heeck, Phys. Lett. B **739,** 256 (2014).

[58] A. Atre, T. Han, S. Pascoli, and B. Zhang, J. High Energy Phys. 05 (2009) 030.

[59] P. Ballett, S. Pascoli, and M. Ross-Lonergan, J. High Energy Phys. 04 (2017) 102.

[60] P. B. Pal and L. Wolfenstein, Phys. Rev. D **25,** 766 (1982).

[61] J. Redondo and M. Postma, J. Cosmol. Astropart. Phys. 02 (2009) 005.